INSTITUTE OF PHYSICS PUBLISHING SMART MATERIALS AND STRUCTURES
Smart Mater. Struct. **13** (2004) 1131–1142 PII: S0964-1726(04)83698-X

A piezoelectric vibration based generator for wireless electronics

S Roundy[1] **and P K Wright**[2]

[1] Department of Engineering, Australian National University, Canberra, ACT 0200, Australia
[2] University of California, Berkeley, 2111 Etcheverry Hall, Berkeley, CA 94720, USA

Received 18 July 2003, in final form 3 June 2004
Published 11 August 2004
Online at stacks.iop.org/SMS/13/1131
doi:10.1088/0964-1726/13/5/018

Abstract
Enabling technologies for wireless sensor networks have gained considerable attention in research communities over the past few years. It is highly desirable, even necessary in certain situations, for wireless sensor nodes to be self-powered. With this goal in mind, a vibration based piezoelectric generator has been developed as an enabling technology for wireless sensor networks. The focus of this paper is to discuss the modeling, design, and optimization of a piezoelectric generator based on a two-layer bending element. An analytical model of the generator has been developed and validated. In addition to providing intuitive design insight, the model has been used as the basis for design optimization. Designs of 1 cm^3 in size generated using the model have demonstrated a power output of 375 μW from a vibration source of 2.5 m s^{-2} at 120 Hz. Furthermore, a 1 cm^3 generator has been used to power a custom designed 1.9 GHz radio transmitter from the same vibration source.

(Some figures in this article are in colour only in the electronic version)

1. Introduction

The vast reduction in size and power consumption of CMOS circuitry has led to a large research effort based around the vision of ubiquitous networks of wireless sensor and communication nodes [1–3]. The wireless devices are usually designed to run on batteries. However, as the networks increase in number and the devices decrease in size, the replacement of depleted batteries becomes impractical. Therefore, alternative methods for powering wireless sensor nodes are needed. Solar power is one alternative power source that has been used to power wireless sensor devices [4]. While solar power is abundant in some applications, it is unsatisfactory in many others.

Mechanical vibrations have received attention from various researchers as a potential source of power for sensors and wireless electronics in a wide variety of applications. Generators based on electromagnetic [5–8], electrostatic [9–11], and piezoelectric [12–16] conversion have been suggested in the literature.

While each type of converter has its benefits for certain kinds of applications, a quick comparison of methods is possible by considering the likely energy density of each type of converter [17]. Such a comparison is given in table 1. From the data in table 1, it appears that piezoelectric generators are capable of producing the highest power output for a given size. This paper will focus on piezoelectric conversion. Further justification for this decision is published elsewhere [17].

Table 1. Summary of maximum energy densities of three kinds of transducers.

Type	Energy density (mJ cm^{-3})	Equation	Assumptions
Piezoelectric	35.4	$(1/2)\sigma_y^2 k^2/2c$	PZT 5 H
Electromagnetic	24.8	$(1/2)B^2/\mu_0$	0.25 T
Electrostatic	4	$(1/2)\varepsilon_0 E^2$	3×10^7 V m^{-1}

σ_y is the yield stress, k is the coupling coefficient, c is the elastic constant, B is the magnetic field, μ_0 is the permeability of free space, ε_0 is the permittivity of free space, and E is the electric field.

Commonly occurring vibration sources, such as HVAC ducts, manufacturing and assembly equipment, and small household appliances, typically range from 0.2 to 10 m s^{-2} in amplitude at frequencies from 60 to 200 Hz [16]. For the

purposes of this paper a vibration source of 2.5 m s^{-2} at 120 Hz has been chosen as a baseline with which to compare generators of differing designs and technologies. This vibration source sits about in the middle of a wide range of low level vibration sources in terms of power output potential, and can thus be considered a representative vibration source.

The purpose of this paper is to investigate the modeling and design of a piezoelectric vibration-to-electricity converter to be used as a power source for wireless electronics. The focus here is on the generator device itself rather than on the associated power electronics. The reader is referred to the work by Ottman *et al* [15] for a discussion of associated power electronics. An analytical model for the generator is first presented. The model is then used to generate design intuition and as a basis for optimal design of the piezoelectric generator. Results are presented that validate the analytical model. Finally, a piezoelectric generator of 1 cm^3 in size is used to power a wireless sensor node.

2. Generator configuration

A target size of 1 cm^3 has been selected based on the size of typical wireless sensor nodes [1]. As will be shown later, the potential power output is directly related to size. Size constraints play an important role in selecting a power converter configuration. For this reason it is necessary to specify the general size at the outset. While the model developed holds for any size, if a generator an order of magnitude larger or smaller were desired, a different design configuration may be preferred.

A bending element has been chosen as the basis for a generator rather than a stack because of the lower resonance frequencies and higher strains attainable. A bending element could be mounted in many ways to produce a generator. A two-layer bender (bimorph) mounted as a cantilever beam with a mass placed on the free end, as shown in figure 1, has been chosen for two reasons. First, for a given force input, the cantilever configuration results in the highest average strain, and the power output is closely related to the average strain developed in the bender. Second, the cantilever mounting results in the lowest resonance frequency for a given size, which is important because the target input vibrations are low frequency (60–200 Hz). Note that in practice there is often a metal shim between the two layers, which is not shown in figure 1.

For the purposes of model development, a beam of uniform width is assumed in order to keep the mathematics more manageable and because benders of uniform width are easily obtainable which makes validation of the model easier. An improvement on the simple cantilever of uniform width can be made by varying the width of the beam. The width can be varied such that the strain along the length of the beam is relatively constant. Thus the average strain can be significantly higher (perhaps close to two times higher) than for a beam of fixed width. The model developed does not lose generality from the assumption of a uniform width beam. The important relationships for design that emanate from the analytical model hold equally well if a beam of non-uniform width is used.

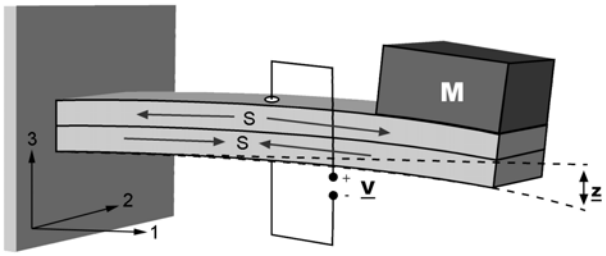

Figure 1. A two-layer bender mounted as a cantilever. S is strain, V is voltage, M is mass, and z is vertical displacement.

3. Basic model

An analytical model of the generator is important not only for estimating the amount of power possible from a given vibration source, but also for making explicit relationships that give the designer of the system some intuition about how to improve its performance. Additionally, the model can be used in conjunction with an optimization routine to optimize geometric design parameters. With these goals in mind, the development of an analytical model for the piezoelectric generator in figure 1 is undertaken.

The established constitutive equations for a linear piezoelectric material in reduced-matrix form are

$$\{S\} = [s^{\mathrm{E}}]\{T\} + [d]^{\mathrm{t}}\{E\} \tag{1}$$

$$\{D\} = [d]\{T\} + [\varepsilon^{\mathrm{T}}]\{E\} \tag{2}$$

where $\{S\}$ is the six-dimensional strain vector, $\{T\}$ is the vector of stresses, $\{D\}$ is the three-dimensional electric displacement vector, $\{E\}$ is the electric field vector, $[s^{\mathrm{E}}]$ is the six by six compliance matrix evaluated at constant electric field, $[d]$ is the three by six matrix of piezoelectric strain coefficients, and $[\varepsilon^{\mathrm{T}}]$ is the three by three dielectric constant matrix evaluated at constant stress. Note that the nomenclature conventions of Tzou [18] are implemented here. Using this convention, T represents the stress induced by the combined mechanical and electrical effects, and σ represents the stress induced by mechanical effects only.

A two-layer bending element mounted as a cantilever beam, as shown in figure 1, is assumed. As is generally the case for bending elements, the material is poled along the 3 axis and electrodes are placed on the surfaces perpendicular to the 3 axis. Driving vibrations are assumed to exist only along the 3 axis. Given these assumptions, the piezoelectric material experiences a one-dimensional state of stress along the 1 axis. Under this stress state, the piezoelectric constitutive equations reduce to the expressions in equations (3) and (4). Note that plane stress formulations have not been considered. While this may lead to small errors, for the beam configuration and dimensions under consideration, these errors are judged not to be very significant.

$$S_1 = s_{11}^{\mathrm{E}} T_1 + d_{31} E_3 \tag{3}$$

$$D_3 = d_{31} T_1 + \varepsilon_3^{\mathrm{T}} E_3. \tag{4}$$

Hereafter $S_1, T_1, D_3, E_3, s_{11}^{\mathrm{E}}$, and $\varepsilon_3^{\mathrm{T}}$ will be written as S, T, D, E, s, and ε for the sake of simplicity. Additionally,

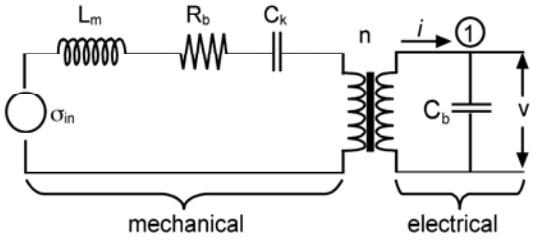

Figure 2. Circuit representation of the piezoelectric generator. (Note that node 1 is used in the derivation of equation (5).)

the elastic constant, $c = s^{-1}$, will generally be used in place of the compliance, s.

A convenient method of modeling piezoelectric elements such that system equations can be easily developed is to model both the mechanical and electrical portions of the piezoelectric system as circuit elements. The electromechanical coupling is then modeled as a transformer [19]. An equivalent circuit for the bender system in figure 1 is shown in figure 2. The equivalent inductor, L_m, represents the mass or inertia of the generator. The equivalent resistor[3], R_b, represents mechanical damping. The equivalent capacitor, C_k, represents the mechanical stiffness. σ_in is an equivalent stress generator that represents the stress developed as a result of the input vibrations. n represents the equivalent turns ratio of the transformer. C_b is the capacitance of the piezoelectric bender. V is the voltage across the piezoelectric device. The 'across' variable on the mechanical side of the circuit is stress, σ (analogous to voltage), and the 'through' variable is strain rate, $\dot{S}$ (analogous to current).

Using this modeling technique, the mechanical side of the circuit is treated as an uncoupled mechanical system. Thus the stress variable used is σ not T, and the stress–strain relationship is $S = s\sigma$ (or $\sigma = cS$). The transformer represents the piezoelectric coupling. Transformers are characterized by a turns ratio that relates voltage on one side to voltage on the other side. In this case, stress on the mechanical side is related to voltage on the electrical side.

As with purely electrical circuits, the system equations are then determined using Kirchhoff's voltage law (KVL) and Kirchhoff's current law (KCL). Taking the sum of 'voltages' around the mechanical side of the circuit yields the expression in equation (5). Summing the currents at node 1 in figure 2 yields the expression in equation (6).

$$\sigma_\mathrm{in} = L_\mathrm{m}\ddot{S} + R_\mathrm{b}\dot{S} + \frac{S}{C_\mathrm{k}} + nV \tag{5}$$

$$i = C_\mathrm{b}\dot{V}. \tag{6}$$

In order for these expressions to be transformed into a usable system model, equivalent expressions for σ_in, L_m, R_b, C_k, n, and i need to be determined.

Figures 3 and 4 contain schematic diagrams of the converter and composite beam showing the geometric variables. Because the piezoelectric bender is a composite

[3] Note that all symbols in the schematic diagram are electrical symbols. Thus the symbol representing mechanical damping, R_b, is a resistor, not a spring. Electrical symbols are used even for mechanical elements in order to make translation to mathematics more consistent and simple.

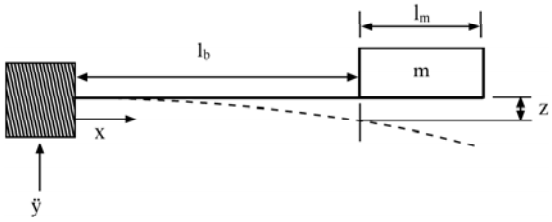

Figure 3. A schematic diagram of the generator.

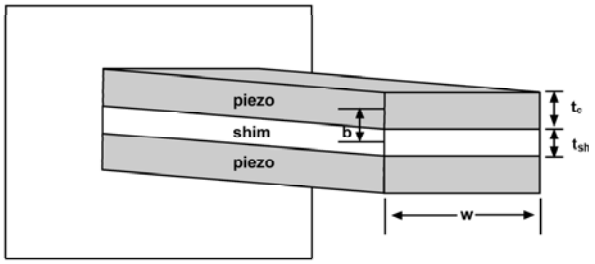

Figure 4. A schematic diagram of the composite beam.

beam, an effective moment of inertia is used. The effective moment of inertia is given by equation (7) below.

$$I = 2\left[\frac{wt_\mathrm{c}^3}{12} + wt_\mathrm{p}b^2\right] + \frac{\eta_\mathrm{s}wt_\mathrm{sh}^3}{12} \tag{7}$$

where w is the width of the beam, η_s is the ratio of the elastic constant of the center shim to that of the piezoelectric material ($\eta_\mathrm{s} = c_\mathrm{sh}/c_\mathrm{p}$ where c_p is the elastic constant for the piezoelectric material and c_sh is the elastic constant for the center shim), and other variables are as shown in figures 3 and 4.

The elastic constant for the piezoelectric ceramic is then used in conjunction with the effective moment of inertia shown by equation (7). The different Young's modulus of the center shim is accounted for by the term η_s in the moment of inertia [20].

The equivalent input stress, σ_in, is a result of the input force, F_in, which is exerted by the proof mass as a direct result of the input vibrations, $\ddot{y}$. Therefore, σ_in can be written as

$$\sigma_\mathrm{in} = k_1 F_\mathrm{in} \tag{8}$$

where k_1 is a geometric constant relating the average stress in the piezoelectric material to force exerted by the mass on the end of the beam. In order to derive an expression for k_1, consider the expression for the average stress in the beam, σ, as shown in equation (9).

$$\sigma = \frac{1}{l_\mathrm{e}}\int_0^{l_\mathrm{e}} \frac{M(x)b}{I}\,\mathrm{d}x \tag{9}$$

where $M(x)$ is the moment, and l_e is the length of the electrode covering the piezoelectric material. The electrode does not necessarily need to extend over the whole length of the beam; however, for the model presented here it will be assumed that $l_\mathrm{e} \leqslant l_\mathrm{b}$. In other words, the electrode does not extend underneath the mass. The expression for the moment is given by

$$M(x) = m(\ddot{y} + \ddot{z})(l_\mathrm{b} + \tfrac{1}{2}l_\mathrm{m} - x). \tag{10}$$

The term $m(\ddot{y}+\ddot{z})$ is really a combination of input force, F_{in}, and inertial force, F_{m}. Substituting $F = F_{\text{in}} + F_{\text{m}} = m(\ddot{y}+\ddot{z})$ into equation (10), equation (10) into (9), and integrating yields the following expression:

$$\sigma = F\frac{b(2l_{\text{b}} + l_{\text{m}} - l_{\text{e}})}{2I}. \tag{11}$$

The constant, k_1, is then

$$k_1 = \frac{b(2l_{\text{b}} + l_{\text{m}} - l_{\text{e}})}{2I}. \tag{12}$$

Remembering that $F_{\text{in}} = m\ddot{y}$, the expression for σ_{in} becomes

$$\sigma_{\text{in}} = k_1 m\ddot{y}. \tag{13}$$

The stress across the 'inductive' element in figure 2 is a result of the inertial force $F_{\text{m}} = m\ddot{z}$. The stress induced by inertial effects can then be written as

$$\sigma_{\text{m}} = k_1 m\ddot{z}. \tag{14}$$

The equivalent inductance of this element, L_{m}, relates stress to the second time derivative of strain (see equation (5) above) rather than displacement as in equation (14). In order to derive the expression for L_{m}, an expression relating average strain, S, to vertical displacement, z, needs to be obtained. Consider the standard beam equation shown in equation (15).

$$\frac{\mathrm{d}^2 z}{\mathrm{d}x^2} = \frac{M(x)}{c_{\text{p}} I} \tag{15}$$

where I is the composite moment of inertia as described by equation (7). Substituting equation (10) into (15) yields

$$\frac{\mathrm{d}^2 z}{\mathrm{d}x^2} = \frac{1}{c_{\text{p}} I} m(\ddot{y}+\ddot{z})\left(l_{\text{b}} + \frac{1}{2}l_{\text{m}} - x\right). \tag{16}$$

Integrating to obtain an expression for the deflection term, z, yields

$$z = \frac{m(\ddot{y}+\ddot{z})}{c_{\text{p}} I}\left(\left(l_{\text{b}} + \frac{1}{2}l_{\text{m}}\right)\frac{x^2}{2} - \frac{x^3}{6}\right). \tag{17}$$

At the point where the beam meets the mass (at $x = l_{\text{b}}$), the expression for z becomes

$$z = \frac{m(\ddot{y}+\ddot{z})l_{\text{b}}^2}{2c_{\text{p}} I}\left(\frac{2}{3}l_{\text{b}} + \frac{1}{2}l_{\text{m}}\right). \tag{18}$$

On substituting $\sigma = c_{\text{p}} S$ and $m(\ddot{y}+\ddot{z}) = F$ into equation (11) above, strain can be written as shown below.

$$S = \frac{m(\ddot{y}+\ddot{z})b}{2c_{\text{p}} I}(2l_{\text{b}} + l_{\text{m}} - l_{\text{e}}). \tag{19}$$

Rearranging equation (19), the force term, $m(\ddot{y}+\ddot{z})$, can be written as shown in equation (20).

$$m(\ddot{y}+\ddot{z}) = \frac{2c_{\text{p}} I}{b(2l_{\text{b}} + l_{\text{m}} - l_{\text{e}})} S. \tag{20}$$

Substituting equation (20) into (18) yields

$$z = S\frac{l_{\text{b}}^2}{3b}\frac{(2l_{\text{b}} + \frac{3}{2}l_{\text{m}})}{(2l_{\text{b}} + l_{\text{m}} - l_{\text{e}})}. \tag{21}$$

Let k_2 be defined as the relationship between z and S as shown in equation (21). The constant k_2 can then be expressed as

$$k_2 = \frac{l_{\text{b}}^2}{3b}\frac{(2l_{\text{b}} + \frac{3}{2}l_{\text{m}})}{(2l_{\text{b}} + l_{\text{m}} - l_{\text{e}})} \tag{22}$$

and $z = k_2 S$. Using this relationship, the displacement term in equation (14) can be replaced with strain. The resulting expression is

$$\sigma_{\text{m}} = k_1 k_2 m\ddot{S}. \tag{23}$$

Referring back to equation (5), L_{m} can now be expressed as in equation (24).

$$L_{\text{m}} = k_1 k_2 m. \tag{24}$$

The resistive element in figure 2 represents damping or mechanical loss. The traditional mechanical damping coefficient, b_{m}, relates force to velocity as shown in equation (25).

$$F_{\text{bm}} = b_{\text{m}}\dot{z}. \tag{25}$$

The equivalent resistance, R_{b}, relates stress (σ) to strain rate ($\dot{S}$). Using the constants k_1 and k_2, force and velocity can easily be replaced with stress and strain rate as shown below.

$$\frac{\sigma_{\text{bm}}}{k_1} = b_{\text{m}} k_2 \dot{S}. \tag{26}$$

The expression for R_{b} is then

$$R_{\text{b}} = k_1 k_2 b_{\text{m}} \tag{27}$$

where the units of b_{m} are the traditional ones: N s m^{-1}.

The capacitive element in figure 2 represents compliance. The equivalent capacitance, C_{k}, relating stress to strain is then simply the compliance constant, s, or the inverse of the elasticity, c_{p}.

Finally, the transformer relates stress (T) to voltage (V) at zero strain [19]. Applying this condition (zero strain) to the piezoelectric constitutive relationship in equation (3) yields the following equation:

$$T = -d_{31} c_{\text{p}} E. \tag{28}$$

The electric field is related to the voltage across the two-layer bender by the following equation:

$$E = \frac{aV}{2t_{\text{c}}} \tag{29}$$

where $a = 1$ if the two layers of the device are wired in series and $a = 2$ if they are wired in parallel. Substituting equation (29) into (28) gives

$$T = \frac{-ad_{31} c_{\text{p}}}{2t_{\text{c}}} V. \tag{30}$$

Equation (30) clearly shows that the equivalent turns ratio, n, for the transformer is

$$n = \frac{-ad_{31} c_{\text{p}}}{2t_{\text{c}}}. \tag{31}$$

The current, i, as shown in figure 2 represents the current generated as a result of the mechanical stress evaluated at zero

electric field. Applying this condition (zero electric field) to equation (4) and substituting strain for stress yields

$$D = d_{31} c_p S. \tag{32}$$

Noting that electrical displacement is nothing more than charge density across a dielectric element, electrical displacement can be related to current for the bender device in figure 1 by

$$i = a w l_e \dot{D}. \tag{33}$$

Substituting equation (33) into (32) yields

$$i = a w l_e d_{31} c_p \dot{S}. \tag{34}$$

It should also be noted that the capacitance of the bender is given by

$$C_b = \frac{a^2 \varepsilon w l_e}{2 t_c}. \tag{35}$$

A usable system model can now be developed by substituting the expressions for σ_{in} (equation (13)), L_m (24), R_b (27), $C_k = c_p^{-1}$, n (31), i (34), and C_b (35) into equations (5) and (6) and rearranging terms. The resulting system equations, in terms of the state variables, S, $\dot{S}$, and V, are

$$\ddot{S} = \frac{-c_p}{k_1 k_2 m} S - \frac{b_m}{m} \dot{S} + \frac{c_p}{k_1 k_2 m} \frac{d_{31} a}{2 t_c} V + \frac{\ddot{y}}{k_2} \tag{36}$$

$$\dot{V} = \frac{2 t_c d_{31} c_p}{a \varepsilon} \dot{S}. \tag{37}$$

The term $c_p/k_1 k_2$ relates force to vertical displacement, which is usually referred to as the equivalent spring constant, k. Substituting k for $c_p/k_1 k_2$, equations (36) and (37) can be written in state space form as shown below:

$$\begin{bmatrix} \dot{S} \\ \ddot{S} \\ \dot{V} \end{bmatrix} = \begin{bmatrix} 0 & 1 & 0 \\ \frac{-k}{m} & \frac{-b_m}{m} & \frac{k d_{31} a}{2 m t_c} \\ 0 & \frac{2 t_c d_{31} c_p}{a \varepsilon} & 0 \end{bmatrix} + \begin{bmatrix} 0 \\ 1/k_2 \\ 0 \end{bmatrix} \ddot{y}. \tag{38}$$

In the development of this model, three important assumptions have been made. First, it was assumed that the mass on the end of the beam acts as a point load located at the center of mass (or halfway along the mass). As a result, provision has not been made for the fact that the slopes of the beam under the mass are identical at all locations. Second, the moment exerted on the beam by the rotational inertia of the proof mass was neglected. This effect is smallest for the fundamental vibration mode, which is the only vibration mode under consideration. Nevertheless, these two assumptions may lead to small errors. Finally, the mass of the beam was neglected. Given the size of the benders and proof masses under consideration (see figures 14 and 15 below), this is a reasonable assumption.

4. Model with resistive load

The model developed in section 3 incorporates no electrical load. Therefore, there is no power transfer. A simple resistive load can be applied in order to estimate how much power can be delivered to a real electrical load. The resulting equivalent circuit diagram is shown in figure 5.

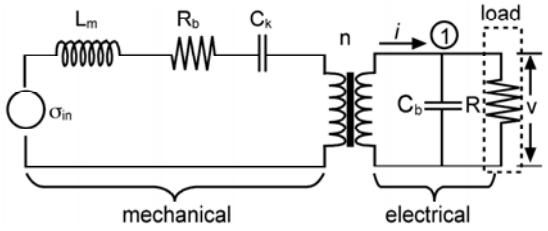

Figure 5. Circuit representation of a piezoelectric generator with a resistive load.

The mechanical side of the equivalent circuit is unchanged, and therefore equations (5) and (36) are unchanged. However, summing the currents at node 1 now yields the following equation in place of equation (6):

$$i = C_b \dot{V} + V/R. \tag{39}$$

The current, i, is still defined by equation (34). Substituting equation (34) into (39) and rearranging terms yields the following equation in place of equation (37):

$$\dot{V} = \frac{2 t_c d_{31} c_p}{a \varepsilon} \dot{S} - \frac{1}{R C_b} V. \tag{40}$$

The resulting system equations in state space form then become

$$\begin{bmatrix} \dot{S} \\ \ddot{S} \\ \dot{V} \end{bmatrix} = \begin{bmatrix} 0 & 1 & 0 \\ \frac{-k}{m} & \frac{-b_m}{m} & \frac{k d_{31} a}{2 m t_c} \\ 0 & \frac{2 t_c d_{31} c_p}{a \varepsilon} & \frac{-1}{R C_b} \end{bmatrix} + \begin{bmatrix} 0 \\ 1/k_2 \\ 0 \end{bmatrix} \ddot{y}. \tag{41}$$

An analytical expression for power transferred to the resistive load can be developed from the model in equation (41). Such an analytical expression is useful not only for estimating power, but also for giving the designer more intuition about the system. The power dissipated by the resistive load is simply V^2/R. Therefore, an analytical expression for V needs to be obtained from equation (41).

Taking the Laplace transform of equation (40) and rearranging terms yields

$$S = \frac{a \varepsilon}{c_p d_{31} t_c s} \left(s - \frac{1}{R C_b} \right) V \tag{42}$$

where s is the Laplace variable, and S and V are used for strain and voltage in both the time and frequency domain. Taking the Laplace transform of equation (36), substituting in the equivalent spring constant k, and rearranging terms yields

$$S \left(s^2 + \frac{b_m}{m} s + \frac{k}{m} \right) = \frac{a k d_{31}}{2 m t_c} V + \frac{A_{in}}{k_2} \tag{43}$$

where A_{in} is the Laplace transform of the input vibrations in terms of acceleration. Substituting equation (42) into (43) and rearranging terms results in the following expression:

$$V \left[s^3 + \left(\frac{1}{R C_b} + \frac{b_m}{m} \right) s^2 + \left(\frac{k}{m} \left(1 + \frac{d_{31}^2 c_p}{\varepsilon} \right) + \frac{b_m}{m R C_b} \right) s + \frac{k}{m R C_b} \right] = \frac{2 c_p d_{31} t_c}{k_2 a \varepsilon} s A_{in}. \tag{44}$$

The expression in equation (44) can be solved for the magnitude of the output voltage. The resulting expression

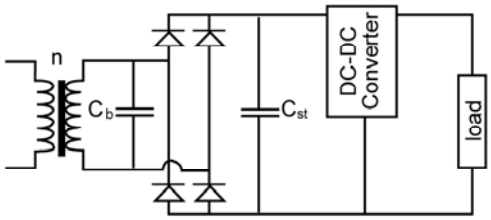

Figure 6. A piezoelectric generator with power circuitry and a load. The equivalent circuit for mechanical elements is not shown.

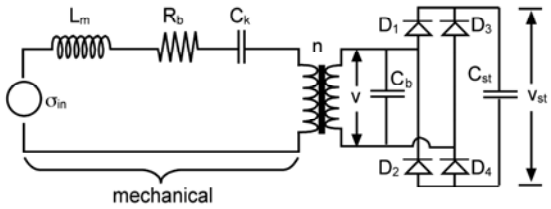

Figure 7. A simplified circuit representation used to analyze the charging of the storage capacitor.

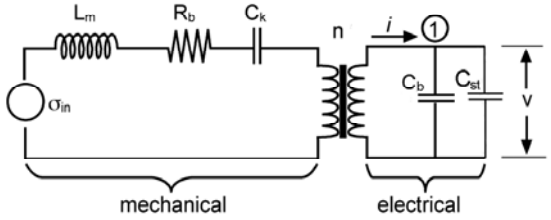

Figure 8. Equivalent circuit representation for state 1, diodes D1 and D4 conducting.

is perhaps more meaningful with the following substitutions: $d_{31}^2 c_p/\varepsilon$ is the square of a term commonly referred to as the piezoelectric coupling coefficient denoted by the symbol k_{31}, the Laplace variable may be replaced with jω where j is the imaginary number, k/m is the natural frequency of the system squared represented by the symbol ω_n^2, and the damping term b_m/m can be rewritten in terms of the unitless damping ratio ζ as $2\zeta\omega_n$. Making these substitutions and solving for V yields

$$V = \left\{ j\omega \frac{2c_p d_{31} t_c}{a\varepsilon} \frac{A_{in}}{k_2} \right\} \left\{ \left[\frac{\omega_n^2}{RC_p} - \left(\frac{1}{RC_b} + 2\zeta\omega_n \right) \omega^2 \right] + j\omega \left[\omega_n^2 (1 + k_{31}^2) + \frac{2\zeta\omega_n}{RC_b} - \omega^2 \right] \right\}^{-1}. \quad (45)$$

If the further simplifying assumption is made that the resonance frequency, ω_n, matches the driving frequency, ω, equation (45) reduces to

$$V = \frac{j\omega \frac{2c_p d_{31} t_c}{a\varepsilon}}{j\omega\left(\omega^2 k_{31}^2 + \frac{2\zeta\omega}{RC_b}\right) - 2\zeta\omega^3} \frac{A_{in}}{k_2}. \quad (46)$$

The rms power transferred to the resistive load is simply $|V|^2/2R$. Therefore, using the expression in equation (46), the resulting analytical term for the rms power transferred to the load is

$$P = \frac{1}{2\omega^2} \frac{RC_b^2 \left(\frac{2c_p d_{31} t_c}{k_2 a\varepsilon}\right)^2 A_{in}^2}{(4\zeta^2 + k_{31}^4)(RC_b\omega)^2 + 4\zeta k_{31}^2 (RC_b\omega) + 4\zeta^2}. \quad (47)$$

The optimal load resistance can then be found by differentiating equation (47) with respect to R, setting the result equal to zero, and solving for R. The resulting optimal load resistance is shown in equation (48).

$$R_{opt} = \frac{1}{\omega C_b} \frac{2\zeta}{\sqrt{4\zeta^2 + k_{31}^4}}. \quad (48)$$

5. Model with capacitive load

The above analysis, based on a simple resistive load, is useful, but it is not a very realistic approximation of the actual electrical load. In reality, the electrical system would look something like the circuit shown in figure 6. The equivalent mechanical side of the circuit is not shown in figure 6, but is exactly the same as in figures 2 and 5. Of course, a rechargeable battery could be used in place of the storage capacitor, C_{st}.

In wireless sensor systems, the radio IC will typically turn on for a short period of time, receive and transmit data, and then turn back off or go into a sleep mode. Typical duty cycles are estimated at around 1% [1]. Therefore, about 99% of the time, the radio IC is in sleep mode and drawing very little current; the DC–DC converter may be shut down during sleep mode as well. Therefore, the vibration converter is just charging up the storage capacitor 99% of the time. A simplified circuit representation for this case is shown in figure 7. The development of a model for this case is useful in that it represents a more realistic operating condition.

There are three possible states in which the circuit shown in figure 7 can operate. State 1 will refer to the state in which diodes D1 and D4 are conducting. State 2 will refer to the state in which diodes D2 and D3 are conducting. And state 3 will refer to the state in which all four rectification diodes are not conducting. An ideal diode model is used in order to simplify the analysis.

In any of the three states, the first system equation, shown above as equation (36), is unchanged. In state 3 (no diodes conducting), the equivalent circuit is the same as that shown in figure 2, and so the second of the two system equations is as shown above in equation (37). The voltage V_{st} is constant in state 3. The equivalent circuit representation for state 1 is shown in figure 8. The second of the two system equations for state 1 is given as equation (49). Note that the storage voltage V_{st} is equal to the voltage across the piezoelectric element, V, in state 1. The second system equation for state 2 is the same as for state 1, equation (49). However, $V_{st} = -V$ in state 2. So, the system model is given by equations (36) and (49) for states 1 and 2, and equations (36) and (37) for state 3.

$$\dot{V} = \frac{a c_p d_{31} l_e w}{C_b + C_{st}} \dot{S}. \quad (49)$$

6. Model for different beam configurations

The utility of developing the constants k_1 and k_2 above is readily evident when considering different beam mounting configurations. The basic model does not change; only the expressions relating average stress to input force (k_1) and average strain to vertical displacement (k_2) are different.

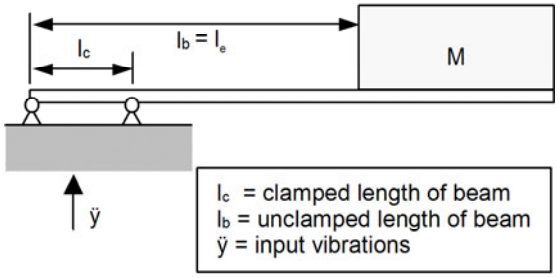

Figure 9. A clamped beam modeled with pin–pin mounting.

Therefore, the models presented as equations (38), (41), and (49) are generally valid for a bender mounted in most beam configurations. However, for each mounting situation, the expressions for k_1 and k_2 will be different. An illustrative example is briefly discussed below.

The model assumes that the mounting structure for the beam is perfectly rigid. In reality, the mounting structure will have some compliance. In practice the benders have been clamped. It was found that, especially for very small (short) designs, a more accurate model for the beam was the pin–pin mounting as shown in figure 9. The length l_c represents the length of the beam under the clamp. It will be further assumed that the length of the electrode, l_e, is equal to the total length of the beam up to the proof mass, l_b. Expressions for k_1 and k_2 are derived in a similar manner to that shown above. The resulting expressions for the pin–pin model are shown as equations (50) and (51). The same models as were derived previously for no load, a resistive load, or a capacitive load can now be applied by simply inserting the new expressions for the constants k_1 and k_2:

$$k_1 = \frac{b(4l_b + 3l_m)}{4I} \tag{50}$$

$$k_2 = \frac{l_b(l_c + l_b)}{3b}. \tag{51}$$

7. Experimental procedure

Experiments were performed to validate the model. Once the model was validated, it was used as the basis for design optimization. Designs were optimized within an overall size constraint of 1 cm^3. Devices with optimized dimensions were then built and tested. Finally, a generator of 1 cm^3 was used to power a custom designed wireless transceiver.

In order to validate the model, both the effective coupling coefficient and mechanical damping ratio were experimentally determined. A prototype generator was made from a two-layer sheet of PZT-5A with a steel center shim. The bimorph, with attached mass (made from a relatively dense alloy of tin and bismuth), is shown in figure 10. The damping ratio was measured by applying an impulse to the system, and then measuring the open circuit voltage output. The resulting damped harmonic oscillation was used to calculate the damping ratio [21]. Several measurements were taken on the device shown in figure 10. The mean value of these measurements was 0.014. This procedure was repeated for each of the devices tested. All of the devices exhibited damping ratios near 0.015.

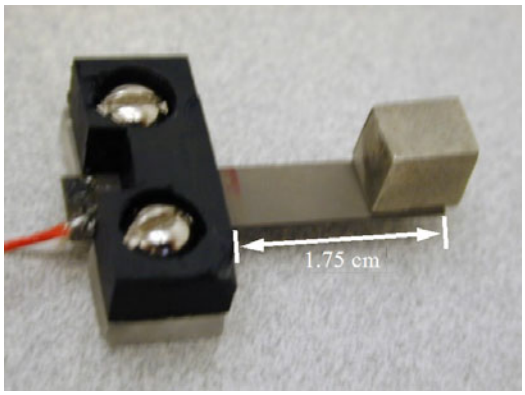

Figure 10. A generator prototype made from PZT-5A.

Figure 11. The piezoelectric generator mounted into a vibrometer used for testing.

The system coupling coefficient was determined by measuring the resonance frequency under open circuit (ω_{oc}) and closed circuit (ω_{sc}) conditions, and applying equation (52) [22]. The coupling coefficient (k_{sys}) of the prototype generator was measured as 0.14.

$$k_{sys}^2 = \frac{\omega_{oc}^2 - \omega_{sc}^2}{\omega_{oc}^2}. \tag{52}$$

The generator prototype was tested by exciting it with vibrations of 2.5 m s^{-2} at 120 Hz. (The generator was designed to resonate at 120 Hz.) The structure was mounted on a vibrometer (Labworks ET-126) as shown in figure 11. The generator prototype was then terminated with a variable resistor, and the voltage across that resistor was measured at various resistances to get voltage magnitude and power transfer versus load resistance data.

Once the model was sufficiently validated, it was used as the basis for optimally selecting dimensions. The output of a dynamic simulation was used as the objective function in conjunction with Matlab's built-in optimization routines. Two

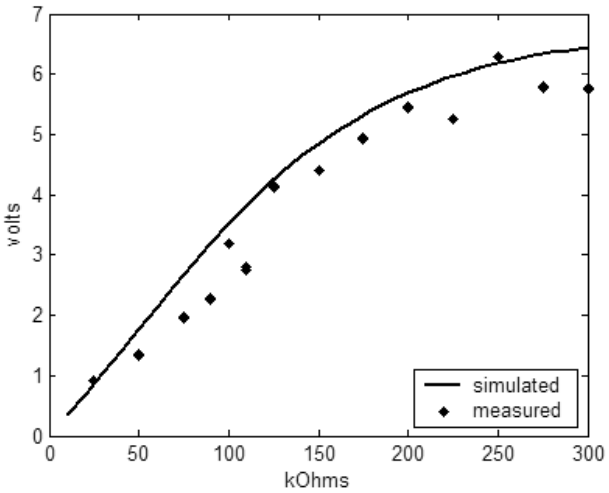

Figure 12. Simulated and measured voltage magnitudes versus load resistance for the prototype device.

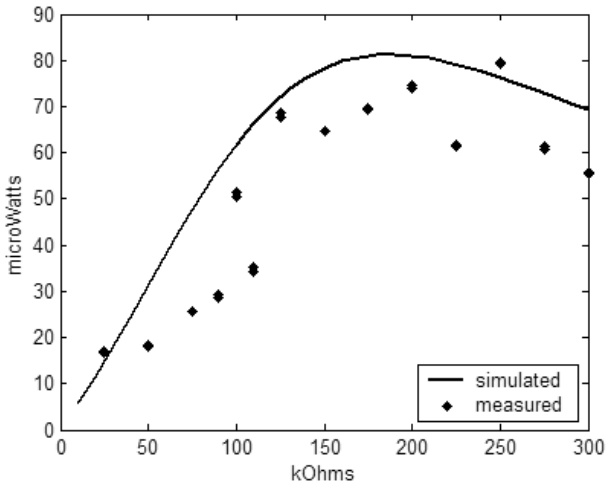

Figure 13. Simulated and measured powers to the resistive load versus resistance for the prototype device.

optimized designs were built and tested with both resistive and capacitive loads. One of these generators was then used to power a custom designed wireless transceiver.

8. Results

The prototype generator shown in figure 10 was excited by vibrations of 2.5 m s^{-2} at 120 Hz. The simulated and measured magnitudes of the voltage across the load resistor as a function of resistance are shown in figure 12. The power transferred to the load resistor is shown in figure 13. Although there is some variability in the measured data, the agreement between experiment and theory was deemed sufficient for using the model as a basis for design optimization.

As mentioned previously, the model was used as a basis for optimizing the design dimensions within an overall size constraint of 1 cm^3. Two designs were built from PZT-5H with a brass center shim purchased from Piezo Systems Inc. The first design, shown in figure 14, had an overall length constraint of 1.5 cm placed on it in addition to the total volume constraint.

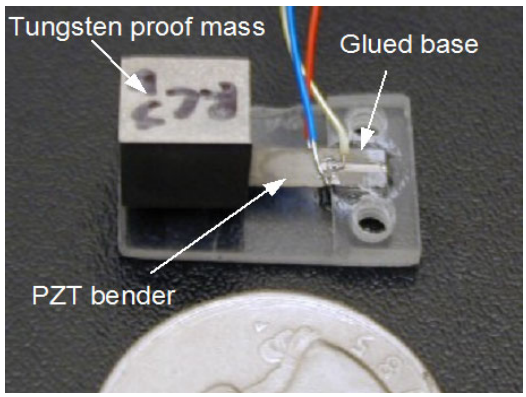

Figure 14. The optimized piezoelectric generator with a 1.5 cm length constraint (design 1).

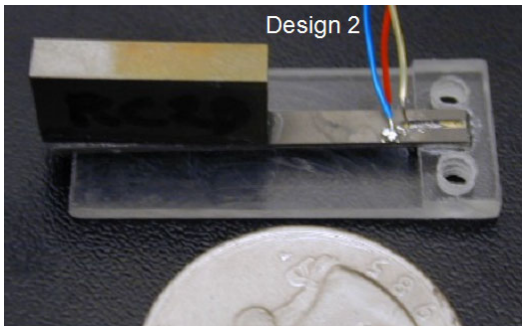

Figure 15. The optimized piezoelectric generator with a 3 cm length constraint (design 2).

Table 2. Dimensions of optimized designs. All dimensions are in mm.

	l_m	h_m	w_m	l	l_e	w	t_p	t_{sh}
Design 1	8.5	7.7	6.7	6.5	6.5	3.2	0.14	0.1
Design 2	17	7.7	3.6	11	11	3.2	0.28	0.1

The length constraint was relaxed to 3 cm for the second design, which is shown in figure 15. The dimensions of each design are shown in table 2. The damping ratios and system coupling coefficients of these structures were also measured. As with the prototype device, the damping ratios were approximately 0.015 and the system coupling coefficients were 0.14. The capacitance of design 1 was 9.2 nF, and the capacitance of design 2 was 8.3 nF. Measured and simulated powers and voltages versus load resistance are shown in figure 16 for the first design and 17 for the second design.

The two designs were also tested with a capacitive load as shown above in figure 7. The devices were driven with baseline vibrations of 2.5 m s^{-2} and the voltage across the storage capacitor was measured as it charged up. The results of these tests are shown in figures 18 and 19. Figure 18 simply shows the voltage across the storage capacitor versus time. The voltage versus time data were used in conjunction with the storage capacitance to calculate the power transfer. Figure 19 shows the power transfer to the storage capacitor versus the ratio of the capacitor voltage to the open circuit voltage of the piezoelectric generator—in other words, the ratio of the instantaneous voltage across the storage capacitor to the maximum voltage to which it will charge in the absence of a

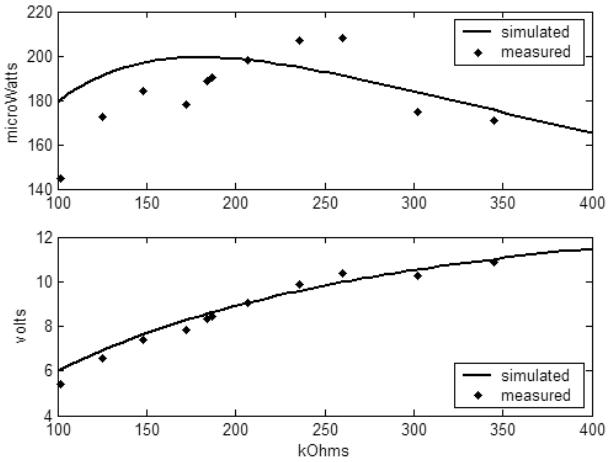

Figure 16. Simulated and measured powers and voltages versus load resistance for design 1.

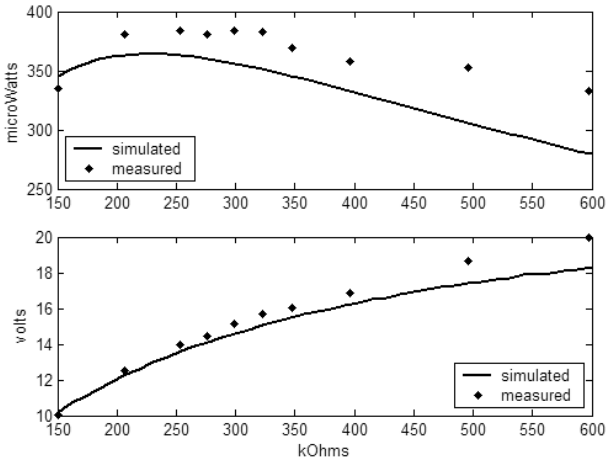

Figure 17. Simulated and measured powers and voltages versus load resistance for design 2.

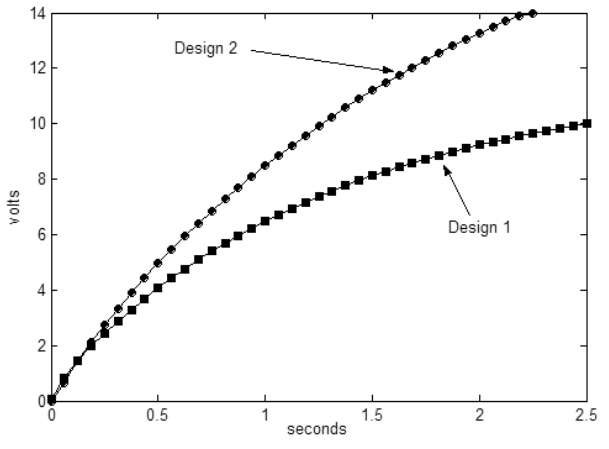

Figure 18. Measured voltage across a 3.3 μF capacitor versus time for the two optimized designs.

load. Because the power transfer is a function of this voltage ratio, this view of the data is more general than viewing the power transfer versus time.

Finally, design 2 was used to power a custom designed radio transmitter [23] from the same baseline input vibrations.

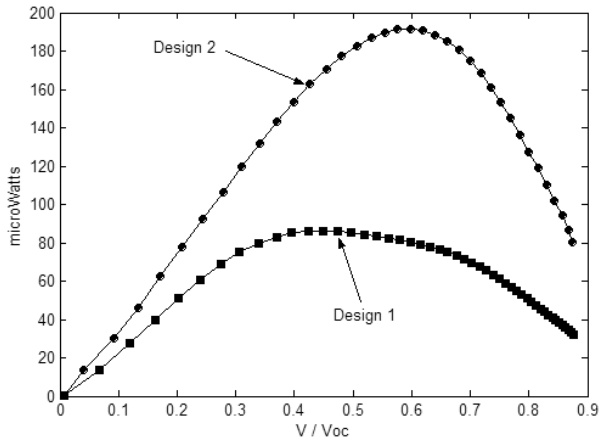

Figure 19. Power transfer to a 3.3 μF storage capacitor versus ratio of capacitor voltage to the open circuit voltage of the piezoelectric generator.

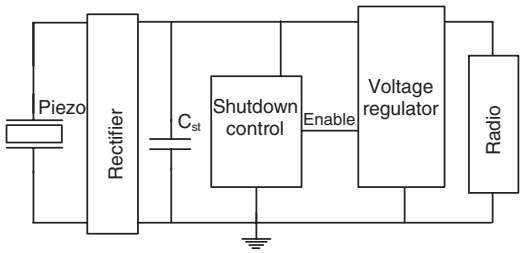

Figure 20. A schematic diagram of the power generation circuit.

A schematic diagram of the entire circuit is shown in figure 20 and a photograph of the physical circuit is shown in figure 21. This power circuit uses a storage capacitor rather than a rechargeable battery. When the storage capacitor charges to a pre-specified energy level, the supply rails to the RF circuitry are activated and energy is consumed. The custom designed radio consumes 10 mA of current at a voltage of 1.2 V when transmitting. The transmit power of the radio is 0 dBm, which gives it an approximate range of 10 m. Because the transmitter dissipates power faster than the piezoelectric bender generates it, the voltage across the storage capacitor falls when the radio is on. Once the energy has been depleted to a level specified by the 'shutdown control' block, the supply rails are disabled and the capacitor is recharged.

Figure 22 shows three measured output voltages from the complete system shown in figures 20 and 21. The top trace shows the voltage across the 47 μF storage capacitor, which discharges as the radio turns on and charges up when it is off. The second trace shows the voltage signal sent out the antennae. Note that the radio is transmitting at 1.9 GHz, which is much faster than the sampling rate for the graph in figure 11. Therefore, some aliasing on the transmission signal has occurred. The bottom trace is the output of the voltage regulator. The regulator also shuts off when the radio is not transmitting. As can be seen in the figure, the storage capacitor discharges much more rapidly than it charges. Using the generator shown above in figure 15 driven by vibrations of 2.5 m s^{-2} in magnitude, the supportable duty cycle was measured as 1.6%.

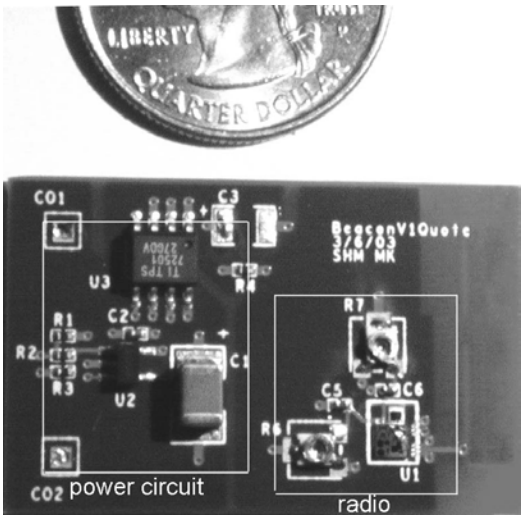

Figure 21. The power circuit and custom designed radio.

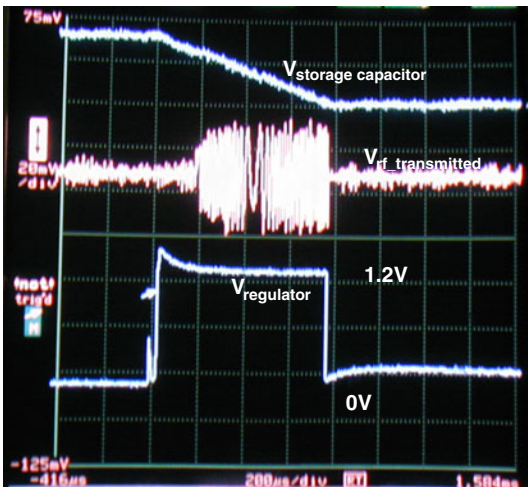

Figure 22. Measured waveforms from the custom radio operating on energy scavenged from vibrations.

9. Discussion

A few important considerations for the designer of a vibration based piezoelectric generator of the type described here should be made clear. First, in the development of the analytical expression for power shown above as equation (47), the assumption that the frequency of the driving vibrations matched the resonance frequency of the system was made. Furthermore, in testing, the driving frequency matched the resonance frequency of the system. Because this resonant system has low damping ($\zeta \sim 0.015$ or $Q \sim 33$), it is essential that the driving frequency match the resonance frequency in order maximize power output. Under many circumstances, the appropriate resonance frequency could be designed. However, in other cases the dominant frequency of the driving vibrations is either unknown, or changing. In these cases, an adaptive structure that can tune its own resonance frequency may be beneficial.

Although it is not exactly clear from the expression for power in equation (47), both experiments and theory show that the power output for a given resonance frequency is linearly proportional to the proof mass attached to the end of the beam. For a given frequency, if the mass is increased, the amount of piezoelectric material will need to increase in order to maintain the resonance frequency. Increasing the amount of material will increase the total strain energy. As it is the total strain energy in the piezoelectric material that is being converted to electrical energy, the electrical power output will also increase. Conversely, if mass is added and the stiffness (or amount of piezoelectric material) is held constant, the resonance frequency will decrease. Assuming that the input vibrations are at this new frequency, the average stress (and strain) in the material, given by equations (9)–(11) above, will increase. Again, the total strain energy increases, and so does the power output. Thus, increasing the mass will always have the effect of increasing the average strain energy, and power output, as long as the assumption of resonance is maintained. Therefore, the designer should try to maximize the mass of the system within size and maximum allowable strain constraints.

Equation (47) shows that power output is inversely related to frequency if the acceleration magnitude of the input vibrations is constant with changing frequency. Therefore, designing the system to resonate at the lower frequency peaks in the vibration spectrum is preferred as long as they have equivalent or higher acceleration magnitude than the higher frequency peaks. Intuitively, if the same level of strain in the piezoelectric material could be maintained at higher frequencies, the power output would increase with frequency. However, this situation would require that the acceleration magnitude of the input vibrations increase with frequency. Equation (47) assumes that the acceleration magnitude is constant with changing frequency. Under this assumption, as the frequency of the design decreases, with the mass constant, the necessary decrease in stiffness will be accompanied by an increase in the level of strain. The converse is also true: the strain level will decrease with increasing frequency, because of the increased stiffness necessary. In practice, the lowest frequency vibration modes from a given source usually have the highest acceleration magnitude. Further data and discussion supporting this statement have been published previously [17].

The electrical load removes energy from the oscillating system, and thus looks like damping to the mechanical system. If a simple resistive load is assumed, this effective damping is related to the resistance of the system. The optimal load resistance shown in equation (48) in effect represents the optimal level of damping for the system. This optimal load resistance is also evident in figures 13, 16, and 17. This concept can be extended to more realistic loads. As shown in figure 18, the power transferred to a capacitive load is maximized when the voltage across the storage capacitor is roughly half the open circuit voltage. This conclusion can be shown by both theory and experimentation, and is in agreement with the findings of Ottman *et al* [15]. For a more detailed description of damping effects in piezoelectric energy scavenging applications, the reader is referred to [24].

Of the two optimized designs presented, the second, longer design exhibits significantly greater output. When the length constraint is relaxed, the optimization routine naturally selects a longer, narrower design. The intuitive explanation for this is that at a given natural frequency, the longer, narrower

design results in a thicker bender with higher average strain from a given input. The power output is closely related to strain and, therefore, the longer narrow design has a higher power output. It will also be noted however, that the long narrow design also results in higher voltage outputs, which may not be desirable in some applications.

The optimization was limited to only a discrete set of bender thicknesses based on what was commercially available. If the optimization routine is allowed to choose an arbitrary thickness, considerable improvement (perhaps up to $2\times$) in power output can be achieved with the same piezoelectric material. This has been verified by simulation, but not by experiment.

It will be noted that the power transfer to a capacitive load was only about half the power transfer to a resistive load under the same excitation. Some of the explanation lies in the fact that the diodes used are not ideal, and do contribute to some power loss. However, the diodes alone cannot account for the entire difference. Work on optimizing the generators for power transfer to capacitive loads is ongoing.

Finally, the design configuration presented in this paper, a two-layer bender mounted as a cantilever beam, has been selected in order to maximize power output from low level vibrations. However, under different circumstances other design configurations may be preferred. For example, if higher level vibrations are present, other design configurations would be more robust while providing only slightly less power for a given volume.

10. Conclusions

As wireless electronics continue to decrease in size and power consumption, the viability of wireless electronic devices powered by ambient vibrations improves. A model for a piezoelectric vibration based generator has been developed. The model has been validated and used not only to estimate power output under a given set of conditions, but also as the basis for generator design optimization. Furthermore, the model provides some design intuition, which is summarized as follows:

(1) The system should be designed to resonate at the dominant driving frequency of the target vibrations if possible.
(2) Power output is proportional to the proof mass attached to the system. Therefore, the proof mass should be maximized while maintaining other constraints such as resonance frequency and strain limits.
(3) Power output is inversely related to the driving and resonance frequency. Therefore, designing for lower frequency peaks in the vibration spectrum is preferred as long as they have equivalent or higher acceleration magnitude than higher frequency peaks.
(4) The energy removed by the electrical load looks like damping to the mechanical system. The load can be designed such that the level of effective electrically induced damping maximizes power transfer to the load.

Two designs have been optimized within an overall space constraint of 1 cm^3. These designs have been built and tested with both resistive and capacitive loads. Experimental results have demonstrated power transfer to a resistive load of 375 μW cm^{-3} from driving vibrations of 2.5 m s^{-2} at 120 Hz. Power transfer to a capacitive load of 190 μW cm^{-3} from the same vibration source has also been demonstrated. Finally, a custom designed radio transceiver that consumes 12 mW when transmitting has been powered at a duty cycle of 1.6% by a 1 cm^3 generator.

Acknowledgments

The authors especially thank Brian Otis and Professor Jan Rabaey at the Berkeley Wireless Research Center (BWRC) for their collaboration and development of the radio transceiver shown in figure 21. The authors gratefully acknowledge the Intel Corporation for support under the Noyce Fellowship, the support of DARPA under grant No F33615-02-2-4005, and the support of the California Energy Commission under contract No 500-01-043.

References

[1] Rabaey J, Ammer J, Karalar T, Li S, Otis B, Sheets M and Tuan T 2002 Picoradios for wireless sensor networks: the next challenge in ultra-low-power design *Proc. Int. Conf. on Solid-State Circuits (San Francisco, CA, Feb. 2002)*
[2] Warneke B, Atwood B and Pister K S J 2001 Smart dust mote forerunners *MEMS 2001: 14th Annual Int. Conf. on Microelectromechanical Systems (Interlaken, Switzerland, Jan. 2001)*
[3] Hill J and Culler D 2002 Mica: a wireless platform for deeply embedded networks *IEEE Micro* **22** 12–24
[4] Roundy S, Otis B P, Chee Y-H, Rabaey J M and Wright P K 2003 A 1.9 GHz RF transceiver beacon using environmentally scavenged energy *ISPLED '03 (Seoul, Korea, Aug. 2003)*
[5] Shearwood C and Yates R B 1997 Development of an electromagnetic micro-generator *Electron. Lett.* **33** 1883–4
[6] Amirtharajah R and Chandrakasan A P 1998 Self-powered signal processing using vibration-based power generation *IEEE J. Solid-State Circuits* **33** 687–95
[7] Ching N N H, Wong H Y, Li W J, Leong P H W and Wen Z 2002 A laser-micromachined multi-modal resonating power transducer for wireless sensing systems *Sensors Actuators* A **97/98** 685–90
[8] El-hami M, Glynne-Jones P, White N M, Hill M, Beeby S, James E, Brown A D and Ross J N 2001 Design and fabrication of a new vibration-based electromechanical power generator *Sensors Actuators* A **92** 335–42
[9] Meninger S, Mur-Miranda J O, Amirtharajah R, Chandrakasan A P and Lang J H 2001 Vibration-to-electric energy conversion *IEEE Trans. Very Large Scale Integr. (VLSI) Syst.* **9** 64–76
[10] Roundy S, Wright P K and Pister K S J 2002 Micro-electrostatic vibration-to-electricity converters *ASME IMECE (New Orleans, LA, Nov. 2002)*
[11] Miyazaki M, Tanaka H, Ono G, Nagano T, Ohkubo N, Kawahara T and Yano K 2003 Electric-energy generation using variable-capacitive resonator for power-free LSI: efficiency analysis and fundamental experiment *ISLPED 2003 (Seoul, Korea, Aug. 2003)*
[12] Schmidt V H 1986 Theoretical electrical power output per unit volume of PVF2 and mechanical-to-electrical conversion efficiency as functions of frequency *Proc. 6th IEEE Int. Symp. on Applications of Ferroelectrics* pp 538–42
[13] Shenck N S and Paradiso J A 2001 Energy scavenging with shoe-mounted piezoelectrics *IEEE Micro* **21** 30–41
[14] Glynne-Jones P, Beeby S P, James E P and White N M 2001 The modelling of a piezoelectric vibration powered generator for microsystems *Transducers 01/Eurosensors XV (June 2001)*

[15] Ottman G K, Hofmann H F and Lesieutre G A 2003 Optimized piezoelectric energy harvesting circuit using step-down converter in discontinuous conduction mode *IEEE Trans. Power Electron.* **18** 696–703
[16] Roundy S, Wright P K and Rabaey J 2003 A Study of low level vibrations as a power source for wireless sensor nodes *Comput. Commun.* **26** 1131–44
[17] Roundy S, Wright P K and Rabaey J M 2003 *Energy Scavenging for Wireless Sensor Networks* (Norwell, MA: Kluwer–Academic)
[18] Tzou H S 1993 Piezoelectric shells *Distributed Sensing and Control of Continua* (Norwell, MA: Kluwer–Academic)
[19] Flynn A M and Sanders S R 2002 Fundamental limits on energy transfer and circuit considerations for piezoelectric transformers *IEEE Trans. Power Electron.* **17** 8–14
[20] Beer F P and Johnston E R 1992 *Mechanics of Materials* (New York: McGraw-Hill)
[21] James M L, Smith G M, Wolford J C and Whaley P W 1994 *Vibration of Mechanical and Structural Systems* (New York: Harper Collins College Publishers)
[22] Lesieutre G A 1998 Vibration damping and control using shunted piezoelectric materials *Shock Vib. Dig.* **30** 187–95
[23] Otis B and Rabaey J 2002 A 300 μW 1.9 GHz CMOS oscillator utilizing micromachined resonators *Proc. 28th European Solid State Circuits Conf. (Florence, Italy, Sept. 2002)*
[24] Lesieutre G A, Hofmann H F and Ottman G K 2002 Structural damping due to piezoelectric energy harvesting *The 13th Int. Conf. on Adaptive Structures and Technologies (Potsdam/Berlin, Germany, Oct. 2002)*